Design and Simulation of a Microelectromechanical Double-Ended Tuning Fork Strain Gauge

A. Bardakas[1], H. Zhang[1], W.D. Leon-Salas[1]
1. School of Engineering Technology, Purdue University, West Lafayette, IN, USA

Abstract
Strain gauges have been extensively used for detecting strain in various applications. Double-ended tuning fork (DETF) strain gages present better performance characteristics than standard foil gauges, including higher sensitivity, smaller size and higher resolution. This study focuses on the design of a microelectromechanical (MEMS) double-ended tuning fork (DETF) and the evaluation of its performance through the comparison of analytical and computational model outcomes. The analytical model predicts the frequency and sensitivity of the gauge using the beam equation while the finite element (FEM) computational model is set up using COMSOL. The analytical and the computational models are in fairly good agreement. The designed MEMS strain gauge has a strain sensitivity of 49.8 Hz/με according to the FEM model and 57.7 Hz/με according to the analytical model. The obtained sensitivity is comparable higher than state-of-the-art MEMS gauges using silicon substrate. Our design has the additional advantage of using a 2-mask SOI process resulting in a simpler fabrication process.

Keywords: Strain gauge, DETF, tuning fork, MEMS.

Introduction

Strain gauges are sensors typically used for measuring strain applied on –man-made or biological structures. Applications of strain gauges range from structural health monitoring of buildings and bridges [1], flexible substrates in mechatronics and [8], to accurate strain measurements in human bone mechanics [9]. In addition, strain measurements can be indirectly used to quantify different phenomena of the system under investigation. Those can be measurement of acceleration, fatigue estimation of engineering structures, torque measurements [4] and mass estimation.

Resistive strain gauges exploit the change in resistance with the application of strain and are usually fabricated using metals and semiconductors. The gauge factor is typically defined as the ratio of the non-dimensional output of the gauge to the strain input. Thus for a resistive gauge the gauge factor (GF) is defined in - (1):

$$GF = \frac{\Delta R / R_0}{\varepsilon} \quad (1)$$

Generally, metallic gauges present a low GF between 2 and 5 while p-type (110) single crystalline silicon (sc-Si) gauges can have a GF as high as 200 [10]. The high GF of silicon gauges, either single crystalline (sc-Si), polycrystalline (Poly-Si) or amorphous is due to the piezoresistive effect along with the ability to modify the gauge resistivity with doping [8].

There are applications that requires a high sensitivity gauge. Depending on the specific setting, there may be additional requirements such as high temperature operation, high temperature or eutectic bonding and high fracture toughness. MEMS-based strain sensors have been demonstrated to be more sensitive than metal or semiconductor gauges [3], be able to withstand high temperatures during operation or bonding [5] while presenting fracture strength of at least 1 GPa.

A DETF resonant strain gauge is presented in [3], used for torque measurements with a sensitivity of 39 Hz/με, including the loss when the sensor is bonded to a substrate. The final sensitivity of the gauge was reported to be 17.5 Hz/με. Additionally, [2] presented a silicon-to-steel induction bonding method verifying the resilience of the gauge to high temperatures while increasing the strain transfer from the substrate to the gauge in comparison to epoxy bonding.

This paper seeks to investigate the performance of a new DETF resonant strain gauge by comparing the analytical model regarding the operation of the sensor with an FEM model constructed in COMSOL 5.2. The analytical modeling treats the resonating tines as linear beams vibrating at their resonant frequency, with the mass of the beam and the actuator modeled as point masses. On the other hand, the FEM model includes the entire device, which allows the effect of the base of the tuning fork and the effect of the anchor to be studied. The device shows high sensitivity at high strains with the analytical and computational models presenting increased difference for strain values above 500 με.

Theory

The Double-Ended Tuning Fork

The double-ended tuning fork geometry consists of several beams, which are resonating to their natural frequency with external excitation. The beams are connected on each end with the base, which is of the same material and usually much stiffer than the beams. The whole structure is suspended by the anchors, which connect the double-ended tuning fork to the substrate. Since it is assumed that the base is much stiffer than the beams, the analysis is focused on one beam viewed as a clamped-clamped one. The differential equation that describes the motion of the beam is [7]:

$$\frac{\partial^2}{\partial x^2}\left(EI\frac{\partial^2 w}{\partial x^2}\right)+\frac{\partial}{\partial x}\left(F\frac{\partial w}{\partial x}\right)+\rho A\frac{\partial^2 w}{\partial t^2}=P(x) \quad (2)$$

where E is the Young's modulus, I the moment of inertia, F the axial force applied on the beam, ρ the density of the beam, P the actuation force applied on the beam and A the cross-section of the beam. The deflection of the beam is given by $w\ (t,\ x)$. The response of the beam at resonance consists of an infinite number of resonating modes. Each mode is independent of one another, consisting of the modal coordinate term, $q_i\ (t)$ and the modal shape $\varphi_i\ (x)$:

$$w(x,t)=\sum_i q_i(t)\phi_i(x) \quad (3)$$

The selected modal shape for this analysis will be the fundamental modal shape of the tuning fork. The solution of the beam equation was presented in [7]. Using this approach, the expressions for the linear spring constant and equivalent mass are shown below [6]:

$$M_{eq,1}=\rho bh\int_0^L \varphi_1{}^2 dx+M_{act}\varphi_1(x_p)^2 \quad (4)$$

$$k_{eq,1}=EI\int_0^L\left(\frac{\partial^2 j_1}{\partial x^2}\right)^2 dx+\frac{1}{2}F\int_0^L\left(\frac{\partial j_1}{\partial x}\right)^2 dx+bhEe_{\text{int}}\int_0^L\left(\frac{\partial j_1}{\partial x}\right)^2 dx \quad (5)$$

where b is the width, h the thickness and L the length of the beam, x_p the position of the actuator mass, M_{act} the mass of the actuator, φ_1 the first oscillation mode and ε_{int} any internal strain residing in the device layer. The natural frequency of the selected mode and thus of the beam is given by:

$$f_r=\frac{1}{2\pi}\sqrt{\frac{k_{eq,1}}{M_{eq,1}}} \quad (6)$$

By substituting equations (4) and (5) into (6), an expression for the resonant frequency as a function of strain ε can be derived:

$$f_r(\varepsilon)=\frac{1}{2\pi}\sqrt{\frac{\frac{256}{15}\frac{Ehb^3}{L^3}+\frac{512}{105}\frac{Ebh\varepsilon}{L}+\frac{512}{105}\frac{Ebh\varepsilon_{\text{int}}}{L}}{\frac{128}{315}\rho bhL+M_{act}}} \quad (7)$$

The length of the beam (L) is 395 µm, the width (b) is 5 µm and the thickness (h) is 10 µm. The device layer will be monocrystalline silicon, thus, the density (ρ) will be 2330 kg/m^3 and the Young's modulus (E) will be 150 GPa. The DETF uses a comb-drive actuator for excitation and sensing with a mass (M_{act}) of 1.77x10^{-10} kg. The comb's drive interdigitated finger gap is 3 µm while the thickness of the fingers is 2 µm. The finger overlap is 15 µm. The frequency sensitivity of the beam can be derived from (7), taking into consideration that the calculation involves both beams. The derived expression for frequency sensitivity of the sensor is given in (8).

$$\frac{\partial f_r}{\partial \varepsilon}=\frac{128Ebh}{105\pi L\left(M_{act}+\frac{128L\rho bh}{315}\right)\sqrt{\frac{\frac{256Eb^3h}{15L^3}}{M_{act}+\frac{128L\rho bh}{315}}}} \quad (8)$$

For simplicity, the internal strain term ε_{int} and the input strain ε term are assumed zero. The sensitivity of the beams to strain greatly depends on their physical dimensions. Thus, the fabrication process needs to accurately reproduce the device geometry. A 0.1 µm increase in the width of the beam results in a 1% decrease in sensitivity. Photolithography tests have shown that the beam and comb drive dimensions can be kept within 0.1 µm. The process selected for the fabrication of the device is the standard silicon-on-insulator (SOI) process, which guaranties that the thickness of the device layer remains unaffected during fabrication and constant at 10 µm. The DETF strain gauge is shown in figure 2.

Numerical Model

Geometric modeling

A parametric FEM model of the DETF mechanism has been created using COMSOL 5.2. Creating the parametric geometry directly in COMSOL allows any changes to the geometry to be readily simulated (without the need to import the geometry from different software) and enables the ability to perform

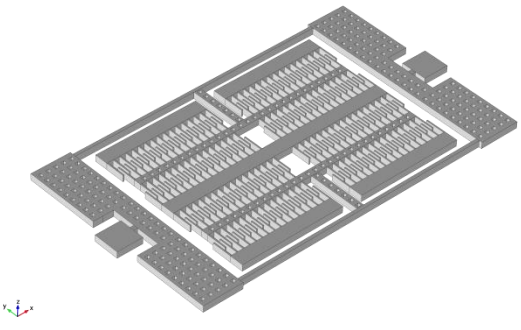

Figure 1. The double-ended tuning fork model.

parametric studies. The 3D geometry consists off the

DETF itself as well as the electrostatic comb drive. The DETF and comb drive dimensions are identical with those used in the analytical formulation. The device is made from a mono-crystalline silicon layer measuring 10 μm in thickness. In addition, a thin 1 μm silicon dioxide layer is located under the anchoring points of the device proving contact with the silicon substrate. The substrate is not modeled in this study. The model of the device is shown in figure 1

Comsol Modeling

The model uses the solid mechanics node and an eigenfrequency analysis in order to calculate the mode shapes of the device. A parametric study was performed to calculate the frequency of the strain gauge at the unstretched position and the frequency shift created by the applied force. The first step of the study was to perform a static analysis according to the applied load and the second is the modal analysis to

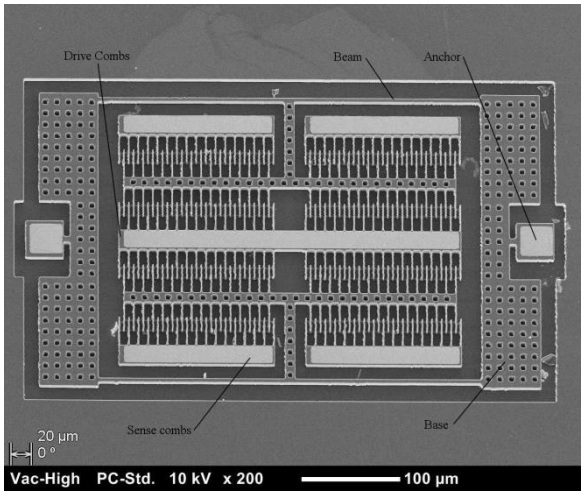

Figure 2. The double-ended tuning fork model through an scanning electron microscope.

estimate the frequency. The force is applied in 0.001 N steps with a maximum of 0.016 N, corresponding to a 0 to 1000 με range. The top surface of the device was meshed using 2D mapped elements and this mesh was swept through the entire volume of the device, resulting in a hexahedral structured mesh. The element size was determined by performing a sensitivity analysis of the mesh. The mesh size was parametrically defined and a modal analysis was performed for each different element size. The final element size was selected based on the difference between consecutive solutions and on the available computational resources. The mesh is shown in figure 3. The maximum element size used to mesh the entire volume was 1.6 μm, yielding 176,616 elements and 5,120,217 degrees of freedom.

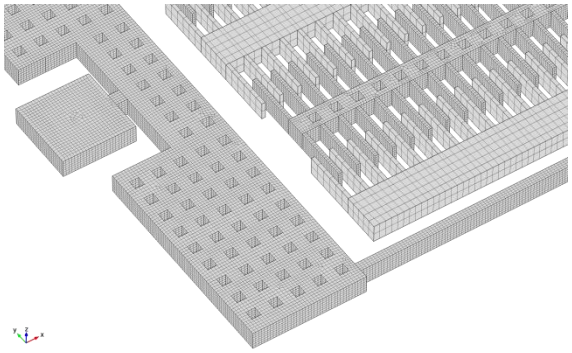

Figure 3. Structured mesh of the model geometry.

The boundary conditions were applied to the bottom of the anchors and to the bottom of the stationary combs, hence a fixed constrain condition. As mentioned before, the SOI process involves a thin silicon dioxide layer between the silicon device layer and bottom silicon layer. Thus, at the bottom of the anchors a 1 μm SiO2 layer was added in order to capture any effects related to the deformation of the anchors. In order to analyze the sensitivity of the sensor, all the degrees of freedom were removed from one of the anchors and a boundary force was applied to the free anchor. The force was applied to the longitudinal direction of the device effectively being a tensile force.

For simulating the electrical behavior of the device under an AC and DC input voltage, the electromechanics node was used and a stationary and frequency domain analysis was performed with harmonic perturbation applied regarding the AC input. The mesh consists of 199,625 tetrahedral elements for a total number of 1,350,582 degrees of freedom. The minimum element size was kept at 10.3 μm due to memory constrains.

The material of the device was modeled as linear elastic material. The fixed constraint condition was applied at the bottom of the anchors and the bottom of the stationary combs, allowing the structure to vibrate. A bias DC voltage was applied at the resonating structure at the 80V level. The AC voltage was applied at the exciting electrode of the comb drive at 0.5V with the harmonic perturbation node. Since the device was intended to operate at atmospheric pressure, the dominant damping mechanism is created from the interaction of the structure with the surrounding air. For a comb drive system, all surfaces in contact with air will contribute to the damping. For this analysis the thin-film damping node was used and the boundary conditions were applied at the bottom of the device and at the comb fingers. The rarefied total accommodation model was used for this study.

Simulation Results

Frequency analysis

In order to find the resonance frequency of the fundamental mode of the beams the modes shapes of the device were modeled and the results are shown in figure 4. The first two modes oscillate in a similar fashion however the difference is that the first one oscillates in a symmetric mode and the second in an antisymmetric one. The antisymmetric mode is preferred due to the fact that the forces on the clamped sides of the beams do not produce a net force on the base.

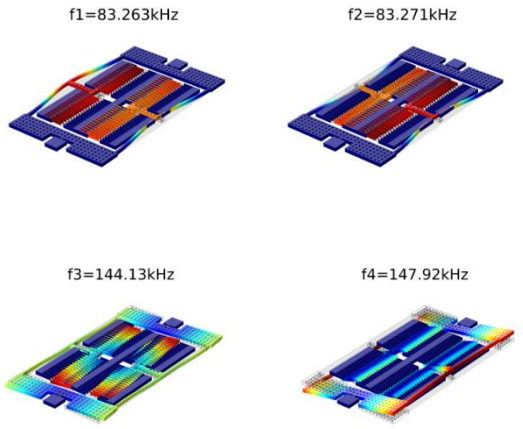

Figure 4. Mode shapes of the double-ended tuning fork structure

The frequency analysis is conducted in order to obtain the maximum amplitude at the resonant frequency at the range of 83.400 to 84.800 kHz with a 60Hz step. The resonant frequency was found to be 84.060 kHz with 1.1 μm maximum displacement of the beams. That frequency is higher than the f2 frequency calculated by the eigenvalue solver. It should be noted that the modal analysis utilized a denser mesh than the frequency analysis. The previous mesh sensitivity analysis showed that the frequency is mesh depended with the frequency increasing linearly with an increasing element size. The frequency response is shown in figure 5.

Strain gauge sensitivity

A comparison of the analytical formulation and the simulation results are shown in figure 6. The unstretched resonant frequency of the gauge predicted by the beam theory was found to be 87.220 kHz and the resonant frequency of the first mode estimated by COMSOL was 83.014 kHz. In this setting, there is no tensile force applied on the beam. Thus, any effects from stretching the beams cannot be held responsible for this 5% difference.

By analyzing the FEM results, it

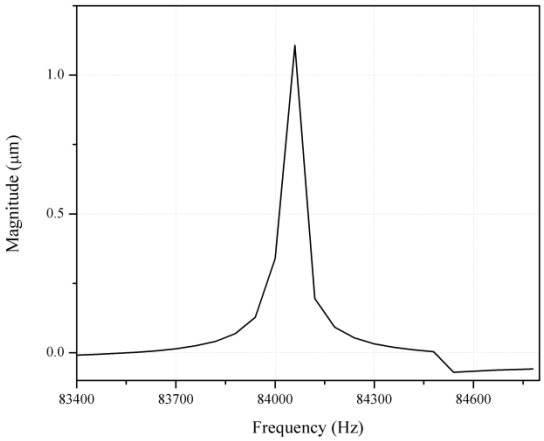

Figure 5. Frequency response of the double-ended tuning fork structure.

seems that when the beams are under oscillation, the base is not rigid enough thus acting as a spring. The same model was recalculated by setting the bases as rigid domains and the unstretched resonant frequency was the same as the analytical one to less than 1%. Therefore, a correction can be applied to the analytical model by taking into account the stiffness of the base.

The sensitivity of the gauge was 57.7 Hz/με, as predicted by (8) taking into account the input strain and 49.8 Hz/με estimated by the FEM model using flexible bases. The two sensitivities are within 10% from 0 to 500 με however at higher strains the difference is greater. This difference is likely due the deformation of the anchor blocks which reduce the sensitivity of the gauge. It should be noted that the calculation of the sensitivity was performed assuming 100% strain transfer from the measurement point to the substrate and from the substrate to the resonating tines. This is the ideal case, and as shown by [3], the sensitivity of the gauge can be reduced as much as 65% due to these inefficiencies.

The strain gauge has been fabricated at the Birck Nanotechnology Center. The fabrication process uses 2 iron oxide masks for the photolithography process. Figure 2 shows a scanning electron microscope image of the fabricated device. The figure shows the comb drives, the beams and other elements of the tuning fork.

Conclusions

This study shows a high sensitivity DETF strain gauge capable of resolving strains as high as 1000 με. By manipulating the dimensions of the gauge it was possible to achieve the high sensitivity without structurally compromising the rest of device. Although the sensitivity of the gauge is higher than other gauges presented in the literature, the strain losses from the substrate and the anchor structure of the DETF have to

be further analyzed. This will provide a more accurate estimation of the gauge output under experimental testing. Additionally, as the device is under fabrication, experimental results will further explain the strain loss mechanism, yielding a better understanding of the gauge performance.

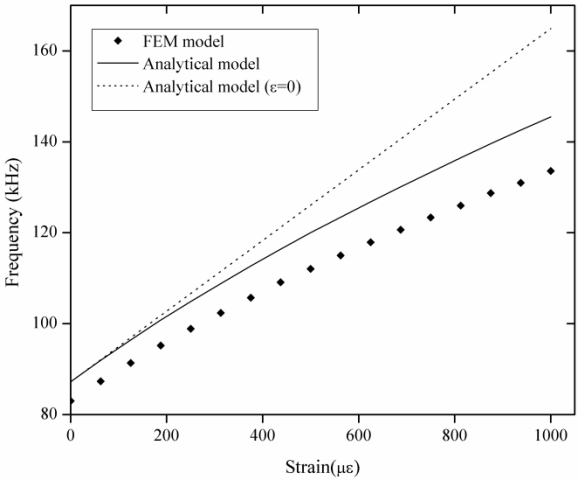

Figure 6. Frequency versus strain showing the difference between the analytical and computational model.

References

1. J. Zhang, S. Guo, Z. Wu and Q. Zhang, "Structural identification and damage detection through lon-gauge strain measurements," *Engineering Structures*, vol. **99**, pp. 173-183, (2015).
2. B. D. Sosnowchik, R. G. Azevedo, D. R. Myers, M. W. Chan, A. P. Pisano and L. Lin, "Rapid silicon-to-steel bonding by induction heating for MEMS strain sensor," *Journal of Microelectromechanical Systems*, vol. **21**, issue 2, pp. 497-506, (2012).
3. D. R. Myers, M. W. Chan, G. Vigevani, B. D. Sosnowchik, R. G. Azevedo, A. V. Jog and A. P. Pisano, "Torque measurements of an automotive halfshaft using micro double-ended tuning fork strain gauges," *Sensors and Actuator, A: Physical*, vol. **204**, pp. 79-87, (2013).
4. D. R. Myers and A. P. Pisano, "Torque measurements of an automotive halfshaft utilizing a MEMS resonant strain gauge," *TRANSDUCERS 2009 – 15th International Conference on Solid-State Sensors, Actuators and Microsystems*, vol. **8**, issue 2, pp. 1726-1729, (2009).
5. D. R. Myers, "MEMS Resonant Strain Sensor Integration," unpublised doctoral dissertation, 2010.
6. A. Fargas-Marques, J. Casals-Terre and A. M. Shkel, "Resonant pull-in condition in parallel-plate electrostatic actuator," *Journal of Microelectromechanical Systems*, vol. **15**, issue 5, pp. 1044-1053, (2007).
7. T. A. W. Roessig, "Integrated MEMS Tuning Fork Oscillators for Sensor Applications," unpublised doctoral dissertation, 1998, UMI: 9902216.
8. Y. Kervran, O. De Sagazan, S. Crand, N. Coulon, T. Mohammed-Brahim and O. Brel, "Microcystaline silicon: Strain gauge sensor arrays on flexible substrate fot the measurement of high deformations," *Sensors and Actuators A: Physical*, vol. **236**, pp. 273-280, (2015).
9. L.Grassi and H. Isaksson, "Extracting accurate strain measuremetns in bone mechanics: A critical review of current methods", *Journal of the mechanical behavior of biomedical materials,* vol. **50**, pp.43-54, (2015).
10. S. Yang and N. Lu, "Gauge factor and stretchability of silicon-on-polymer gauges", *Sensors*, vol. **13**, issue 7, pp. 8577-8594, (2013).

Acknowledgements

The author would like to thank the Center for Technology Development (CTD) as well as AAM, Deere, Eaton and Faurecia for supporting and sponsoring this project.